Received November 11, 2019, accepted November 24, 2019, date of publication December 2, 2019, date of current version December 16, 2019.

Digital Object Identifier 10.1109/ACCESS.2019.2956783

Analysis of a Novel Two-Lane Lattice Hydrodynamic Model Considering the Empirical Lane Changing Rate and the Self-Stabilization Effect

TING WANG, RONGJUN CHENG, AND HONGXIA GE
Faculty of Maritime and Transportation, Ningbo University, Ningbo 315211, China
Jiangsu Province Collaborative Innovation Center for Modern Urban Traffic Technologies, Nanjing 210096, China
National Traffic Management Engineering and Technology Research Centre, Ningbo University Sub-Centre, Ningbo 315211, China

Corresponding author: Rongjun Cheng (chengrongjun@nbu.edu.cn)

This work was supported in part by the National Natural Science Foundation of China under Grant 71571107, in part by the National Key Research and Development Program of China-Traffic Modeling, Surveillance, and Control with Connected and Automated Vehicles under Grant 2017YFE9134700, and in part by the K. C. Wong Magna Fund in Ningbo University, China.

ABSTRACT Considering the impact of the empirical lane changing rate and self-stabilization effect on traffic flow stability synthetically, an extended two-lane lattice hydrodynamic model was proposed in this paper. In the first place, the stability condition is acquired through applying liner stability analysis method and it reveals that both the empirical lane changing rate and self-stabilization effect can enhance the stability of traffic flow to some extent. Next, in order to analyze the transmission mechanism of traffic congestion, the modified Korteweg-de Vries (mKdV) equation is deduced by using nonlinear theory near the critical point. At the same time, the kink-antikink solitary wave solution is obtained to describe the propagation behavior of traffic density wave by solving the mKdV equation. Subsequently, the numerical simulations are carried out and the results coincide well with the theoretical analysis, which indicate the empirical lane changing rate and the self-stabilization effect can improve the traffic stability.

INDEX TERMS Traffic flow, lattice hydrodynamic model, the empirical lane changing rate, the self-stabilization effect.

I. INTRODUCTION

Urban roads are the lifeblood of urban traffic, and the smoothness of roads has an important impact on urban traffic conditions. But now, the continuous increase of vehicle ownership seriously affects the road driving environment. The following problems, such as the deterioration of urban environment, the decline of urban vitality and the prominent contradiction between people and vehicles, have prompted many scholars to think deeply about traffic congestion. In fact, it is very important and effective to explore the nonlinear phenomenon of traffic flow and reveal its essential characteristics. What's more, modeling can help scholars visualize the traffic flow system according to the actual situation. Hence, a lot of scholars have considered and established many traffic flow models [1]–[25] to analyze and explore the features of traffic flow, such as micro models [4]–[14], macro models [15]–[19] and lattice hydrodynamic models [20]–[23]. These models not only enrich and develop traffic flow theory, but also provide a lot of new ideas for many traffic engineering practices.

The first thing to introduce is that Nagatani [24] pointed out the earliest lattice hydrodynamic model in 1998, which believed that the traffic flow can be optimized by the product of the optimal velocity and the average density. For the purpose of relating to the actual traffic environment, many extended lattice hydrodynamic models [25]–[29] have been raised up by pondering a series of factors encountered in the progress of driving, such as honk effect [25], anticipation effect [26], density difference effect [27] and so on. In general, these models are helpful for improving traffic efficiency and reducing traffic congestion. At the same time, the improvement and enrichment of traffic flow models will also promote the development of the traffic flow theory. One year later, in 1999, Nagatani [30] expanded single-lane lattice

The associate editor coordinating the review of this manuscript and approving it for publication was Zheng Chen.

hydrodynamic into two-lane lattice hydrodynamic model, which analyzed and concluded the positive influence of lane changing on traffic flow stability. Gradually, some scholars think that constant lane changing rate can't adequately reflect the actual traffic. In 2019, Zhu *et al.* [31] replaced the previous commonly used constant lane changing rate with empirical lane changing rate, and he believed that the use of this lane changing rate was more convincing for the analysis and research of two-lane lattice hydrodynamic model.

Besides, in 2018, inspired by the Li's [33] consideration of the self-stabilization in car-following model, Zhang [34] proposed an extended lattice hydrodynamic model by thinking over the self-stabilization effect of lattice's historical flow. Subsequently, Peng *et al.* [35] found that this factor was not taken into account in the presence of lane changing behavior, so he developed a modified two-lane lattice hydrodynamic model to explore how the self-stabilization effect of current lattice's historical flow affect the traffic flow stability. If we consider the self-stabilization effect in the case of empirical lane changing rate, it will make the model more consistent with the actual traffic situation, and the model can also provide a theoretical reference for the actual traffic governance. Therefore, we establish a novel two-lane lattice hydrodynamic model considering the empirical lane changing rate and the self-stabilization effect.

The remainder of our article is structured as follows. In Section 2, we describe the process and results of linear stability analysis for the new model. Later in Section 3, we make use of the nonlinear analysis to deduce the mKdV equation successfully. Next, in order to verify the feasibility of the new model, numerical simulations are performed, and the results are exactly consistent with the previous theoretical analysis results. At last, we give a reasonable conclusion in Section 6.

II. THE MODIFIED LATTICE HYDRODYNAMIC MODEL

In 1999, Nagatani [30] postulated that when there is a density difference between two lanes, vehicles will change lane, then he put forward the first two-lane lattice hydrodynamic model. And the schematic of the traffic flow's basic situation on two-lane road is shown in Fig.1 below. It means that when the density at site j on lane 1 is lower than the density at site $j-1$ on lane 2, vehicles divert from lane 2 to lane 1 and the lane changing rate is $\gamma\left|\rho_0^2V'(\rho_0)\right|\left(\rho_{2,j-1}-\rho_{1,j}\right)$. In the same way, when the density at site j on lane 1 is higher than site $j+1$ on lane 2, the lane changing happens from the lane 1 to the lane 2, and lane changing rate is $\gamma\left|\rho_0^2V'(\rho_0)\right|\left(\rho_{1,j}-\rho_{2,j+1}\right)$. Therefore, Nagatani [30] got the following continuity equations of lane 1 and lane 2 respectively:

$$\begin{aligned}&\partial_t\rho_{1,j}+\rho_0\left(\rho_{1,j}v_{1,j}-\rho_{1,j-1}v_{1,j-1}\right)\\&\quad=\gamma\left|\rho_0^2V'(\rho_0)\right|\left(\rho_{2,j+1}-2\rho_{1,j}+\rho_{2,j-1}\right)\end{aligned}\tag{1}$$

$$\begin{aligned}&\partial_t\rho_{2,j}+\rho_0\left(\rho_{2,j}v_{2,j}-\rho_{2,j-1}v_{2,j-1}\right)\\&\quad=\gamma\left|\rho_0^2V'(\rho_0)\right|\left(\rho_{1,j+1}-2\rho_{2,j}+\rho_{1,j-1}\right)\end{aligned}\tag{2}$$

where $\rho_{1,j}$ and $\rho_{2,j}$ represent the densities on lane 1 and lane 2, respectively.

Then, through adding Eq. (1) and Eq. (2), the continuity equation of two-lane model is deduced as below

$$\partial_t\rho_j+\rho_0\left(\rho_jv_j-\rho_{j-1}v_{j-1}\right)=\gamma\left|\rho_0^2V'(\rho_0)\right|\left(\rho_{j+1}-2\rho_j+\rho_{j-1}\right)\tag{3}$$

where $\rho_j=\frac{\rho_{1,j}+\rho_{2,j}}{2}$, $\rho_jv_j=\frac{\rho_{1,j}v_{1,j}+\rho_{2,j}v_{2,j}}{2}$, $V\left(\rho_j\right)=\frac{V(\rho_{1,j})+V(\rho_{2,j})}{2}$, the average density is expressed as ρ_0, $\rho_j$and v_j denote the local density and velocity at site j on lanes, respectively, γ indicates the rate constant coefficient.

Recently, according to the measured datasets of lane changing rate in real traffic environment, Zhu *et al.* [31] proposed an extended model by taking the empirical lane changing rate into account, which is more reasonable compared with the previous fixed lane changing rate. And the empirical lane changing rate applying the form of the Lee optimal velocity [32], which is expressed as follows:

$$\gamma(\rho)=\gamma_{\max}\frac{1-\rho/\rho_m}{1+E\left(\rho/\rho_m\right)^4}\tag{4}$$

where $\gamma_{\max}$ means the maximum coefficient of lane changing rate and ρ_m represents the maximum density, besides, E is a constant.

What's more, after analyzing the datasets, Zhu *et al.* [31] defined the lane changing rate depends on the density of the former lattice site. The concrete manifestations are as follows: if the site $j-1$ on lane 2 has a higher density than site j on lane 1, there will be a phenomenon of vehicles changing from lane 2 to lane 1, and the lane changing rate is expressed as $\gamma\left(\rho_j\right)\left|\rho_0^2V'(\rho_0)\right|\left(\rho_{2,j-1}-\rho_{1,j}\right)$; if the density at site j on lane 1 is higher than site $j+1$ on lane 2, vehicles will transfer from lane 1 to lane 2, and the lane changing rate is written as $\gamma\left(\rho_j\right)\left|\rho_0^2V'(\rho_0)\right|\left(\rho_{1,j}-\rho_{2,j+1}\right)$.

Therefore, the continuity equations of lane 1 and lane 2 can be changed to the following forms:

$$\begin{aligned}&\partial_t\rho_{1,j}+\rho_0\left(\rho_{1,j}v_{1,j}-\rho_{1,j-1}v_{1,j-1}\right)\\&\quad=\left|\rho_0^2V'(\rho_0)\right|\left[\gamma\left(\rho_j\right)\left(\rho_{2,j-1}-\rho_{1,j}\right)-\gamma\left(\rho_{j+1}\right)\right.\\&\qquad\left.\times\left(\rho_{1,j}-\rho_{2,j+1}\right)\right]\end{aligned}\tag{5}$$

$$\begin{aligned}&\partial_t\rho_{2,j}+\rho_0\left(\rho_{2,j}v_{2,j}-\rho_{2,j-1}v_{2,j-1}\right)\\&\quad=\left|\rho_0^2V'(\rho_0)\right|\left[\gamma\left(\rho_j\right)\left(\rho_{1,j-1}-\rho_{2,j}\right)-\gamma\left(\rho_{j+1}\right)\right.\\&\qquad\left.\times\left(\rho_{2,j}-\rho_{1,j+1}\right)\right]\end{aligned}\tag{6}$$

Combining Eq. (5) and Eq. (6), the two-lane traffic's continuity equation can be obtained as below:

$$\begin{aligned}&\partial_t\rho_j+\rho_0\left(\rho_jv_j-\rho_{j-1}v_{j-1}\right)\\&=\left|\rho_0^2V'(\rho_0)\right|\left[\gamma\left(\rho_j\right)\left(\rho_{j-1}-\rho_j\right)-\gamma\left(\rho_{j+1}\right)\left(\rho_j-\rho_{j+1}\right)\right]\end{aligned}\tag{7}$$

where $\rho_jv_j=\frac{\rho_{1,j}v_{1,j}+\rho_{2,j}v_{2,j}}{2}$.

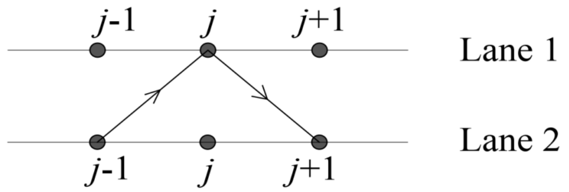

FIGURE 1. The basic situation of traffic flow on two-lane straight road.

In addition, since the evolution equation for two-lane model doesn't change with the occurrence of lane changing behavior, it is written in the following form:

$$\partial_t \rho_j(t) v_j(t) = a\rho_0 V\left(\rho_{j+1}(t)\right) - a\rho_j(t) v_j(t) \tag{8}$$

where a is driver's sensitivity, $V\left(\rho_j(t)\right)$ means the optimal velocity function, which is adopted as follows:

$$V\left(\rho_j(t)\right) = \frac{v_{\max}}{2}\left[\tanh\left(\frac{2}{\rho_0} - \frac{\rho_j(t)}{\rho_0^2} - \frac{1}{\rho_c}\right) + \tanh\left(\frac{1}{\rho_c}\right)\right] \tag{9}$$

Likewise, in 2019, Peng *et al.* [35] explored the effect of self-stabilization caused by the current lattice's historic flux on traffic stability in two-lane lattice model, and the evolution equation is described as below:

$$\begin{aligned}\partial_t \rho_j(t) v_j(t) &= a\rho_0 V\left(\rho_{j+1}(t)\right) - a\rho_j(t) v_j(t) \\ &\quad + \lambda a\left[\rho_j(t) v_j(t) - \rho_j(t-\tau_0) v_j(t-\tau_0)\right]\end{aligned} \tag{10}$$

where τ_0 indicates the historical time and the coefficient corresponding to the self-stabilization effect is denoted as λ. However, the influences of self-stabilization effect and the empirical lane changing rate has not been analyzed simultaneously in the two-lane lattice models so far. Thus, we establish the modified model by means of eliminating the velocity in Eq. (7) and Eq. (10), and we finally acquire the following evolution equation of traffic density:

$$\begin{aligned}&\partial_t^2 \rho_j + a\rho_0^2\left[V\left(\rho_{j+1}\right) - V\left(\rho_j\right)\right] + (1-\lambda)\, a\partial_t \rho_j \\ &\quad - (1-\lambda)\, a\left|\rho_0^2 V'(\rho_0)\right|\begin{bmatrix}\gamma\left(\rho_j\right)\left(\rho_{j-1} - \rho_j\right) \\ -\gamma\left(\rho_{j+1}\right)\left(\rho_j - \rho_{j+1}\right)\end{bmatrix} \\ &\quad + \lambda a\partial_t \rho_j(t-\tau_0) - \lambda a\left|\rho_0^2 V'(\rho_0)\right| \\ &\quad \times \begin{bmatrix}\gamma\left(\rho_j(t-\tau_0)\right)\left(\rho_{j-1}(t-\tau_0) - \rho_j(t-\tau_0)\right) \\ -\gamma\left(\rho_{j+1}(t-\tau_0)\right)\left(\rho_j(t-\tau_0) - \rho_{j+1}(t-\tau_0)\right)\end{bmatrix} \\ &\quad - \left|\rho_0^2 V'(\rho_0)\right|\partial_t\left[\gamma\left(\rho_j\right)\left(\rho_{j-1} - \rho_j\right)\right. \\ &\quad \left. - \gamma\left(\rho_{j+1}\right)\left(\rho_j - \rho_{j+1}\right)\right] = 0\end{aligned} \tag{11}$$

III. LINEAR STABILITY ANALYSIS

In order to obtain the stability condition of traffic flow, we apply linear analysis method to study the modified model we proposed. And we introduce a small disturbance into the traffic flow system. As we can know, the degree of disturbance will continue to increase with the spread of the traffic flow when the traffic system is unstable. On the contrary, if the traffic system is stable, the disturbance will decrease gradually until stabilize in a minimal range.

Distinctly, the following condition satisfy the equilibrium solution of Eq. (11) in uniform traffic flow:

$$\rho_j(t) = \rho_0,\, v_j(t) = V(\rho_0) \tag{12}$$

Supposing a small perturbation deviating from the stead-state solution expressed as y_j at site j, which would cause the density at site j to be rewritten in the following form:

$$\rho_j(t) = \rho_0 + y_j(t) \tag{13}$$

Then, substituting Eq. (13) into Eq. (11), we can obtain:

$$\begin{aligned}&\partial_t^2 y_j(t) + a\rho_0^2 V'(\rho_0)\left(y_{j+1} - y_j\right) + \lambda a\partial_t y_j(t-\tau_0) \\ &\quad - \left|\rho_0^2 V'(\rho_0)\right|\gamma(\rho_0)\left(\partial_t y_{j+1} - 2\partial_t y_j + \partial_t y_{j-1}\right) \\ &\quad + (1-\lambda)\, a\partial_t y_j(t) - (1-\lambda)\, a\left|\rho_0^2 V'(\rho_0)\right| \\ &\quad \times \gamma(\rho_0)\left(y_{j-1} - 2y_j + y_{j+1}\right) \\ &\quad - \lambda a\left|\rho_0^2 V'(\rho_0)\right|\gamma(\rho_0)\left[y_{j-1}(t-\tau_0) - 2y_j(t-\tau_0)\right. \\ &\quad \left. + y_{j+1}(t-\tau_0)\right] = 0\end{aligned} \tag{14}$$

where $V'(\rho_0) = \frac{\partial V(\rho)}{\partial \rho}\Big|_{\rho=\rho_0}$.

Next, expanding y_j into Fourier series, that is, letting $y_j(t) = \exp(ikj + zt)$, where i is imaginary number, k is a parameter deciding the shape of the perturbation, j is the number of the lattice, and z is a complex variable to be determined, t means the time. Then substituting it into Eq. (14) to get the Eq. (15) written as follows:

$$\begin{aligned}&z^2 + a\rho_0^2 V'(\rho_0)\left(e^{ik} - 1\right) + (1-\lambda)\, az \\ &\quad - \lambda a\left|\rho_0^2 V'(\rho_0)\right|\gamma(\rho_0)\left(e^{-ik-z\tau_0} - 2e^{-z\tau_0} + e^{ik-z\tau_0}\right) \\ &\quad + \lambda aze^{-z\tau_0} \\ &\quad - (1-\lambda)\, a\left|\rho_0^2 V'(\rho_0)\right|\gamma(\rho_0)\left(e^{-ik} - 2 + e^{ik}\right) \\ &\quad - \left|\rho_0^2 V'(\rho_0)\right|\gamma(\rho_0)\left(ze^{-ik} - 2z + ze^{ik}\right) = 0\end{aligned} \tag{15}$$

For simplicity, letting $z = z_1(ik) + z_2(ik)^2 + \cdots$ and substituting it into Eq. (15), and the first and second order terms of ik can be deduced as follows:

$$z_1 = -\rho_0^2 V'(\rho_0) \tag{16}$$

$$z_2 = -\left[\begin{array}{l}\dfrac{\rho_0^4 V'(\rho_0)^2}{a} + \dfrac{\rho_0^2 V'(\rho_0)}{2} \\ -\left|\rho_0^2 V'(\rho_0)\right|\gamma(\rho_0) - \lambda\tau_0\rho_0^4\left(V'(\rho_0)^2\right)\end{array}\right] \tag{17}$$

Based on the traffic flow stability theory and the above derived results, we know that when $z_2 < 0$, the steady-state flow becomes unstable. On the contrary, when $z_2 > 0$, the traffic flow system would maintain stable. In other words, the stability conditions have been met. As a result, we can get the neutral stability condition as below:

$$a = \frac{-2\rho_0^2 V'(\rho_0)}{1 + 2\gamma(\rho_0) - 2\lambda\tau_0\rho_0^2 V'(\rho_0)} \tag{18}$$

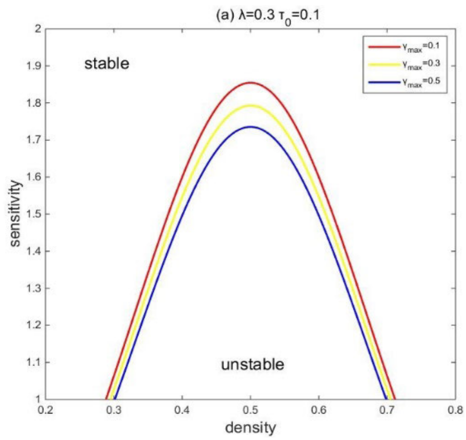

FIGURE 2. The neutral stability curves for $\gamma_{\max} = 0.1, 0.3, 0.5$ with $\lambda = 0.3$ and $\tau_0 = 0.1$.

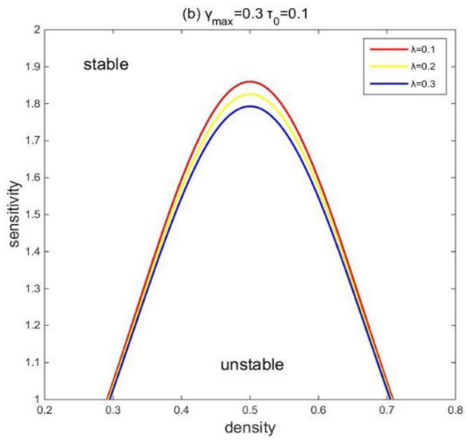

FIGURE 3. The neutral stability curves for $\lambda = 0.1, 0.2, 0.3$ with $\gamma_{\max} = 0.3$ and $\tau_0 = 0.1$.

Consequently, the stability condition for uniform traffic flow is

$$a > \frac{-2\rho_0^2 V'(\rho_0)}{1 + 2\gamma(\rho_0) - 2\lambda\tau_0\rho_0^2 V'(\rho_0)} \tag{19}$$

The neutral stability curves under different parameters are shown in the following Fig.2, Fig.3 and Fig.4. As shown in the figure, the upper region of the curve is the stable region, whereas the lower part of the curve is an unstable region.

Fig.2 is drawn by setting the different $\gamma_{\max}$ with $\lambda = 0.3$ and $\tau_0 = 0.1$.When $\gamma_{\max} = 0.5$, the corresponding curve appears at the bottom. Besides, it's obvious for us to find that the vertices of neutral stability curves move downward as the $\gamma_{\max}$ increases, which send out a message that increasing $\gamma_{\max}$ can enhance the traffic flow stability. Fig.3 is the result of setting different λ under the premise that $\gamma_{\max}$ and τ_0 are fixed equal to 0.3 and 0.1 respectively. Similarly, we can clearly note that with the increasing of λ, the area of the stability region is increasing, which shows that the self-stabilization has a certain role in relieving traffic pressure. What reveals from Fig.4 is that curve decreases continuously with the historical time τ_0 increases from 0.1 to 0.3, which announces that the historical time τ_0 promotes traffic flow stability.

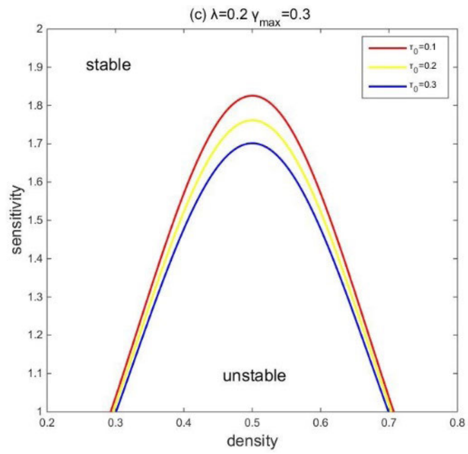

FIGURE 4. The neutral stability curves for $\tau_0 = 0.1, 0.2, 0.3$ with $\lambda = 0.2$ and $\gamma_{\max} = 0.3$.

IV. NONLINEAR ANALYSIS

In order to analyze the nonlinear phenomena of traffic flow, we consider the behavior of spatial and temporal slow variables near the critical point (ρ_c, a_c) in the unstable region of traffic flow, which are specified in the following form:

$$X = \varepsilon(j + bt), \quad T = \varepsilon^3 t, \ 0 < \varepsilon \ll 1 \tag{20}$$

where b means the undetermined parameters. Then we set the density of each lattice $\rho_j(t)$ to

$$\rho_j(t) = \rho_c + \varepsilon R(X, T) \tag{21}$$

According to the above Eq. (20) and Eq. (21), using the Taylor expansion method, each item in Eq. (11) is expanded to the fifth term of ε, then we can get the following expression:

$$\begin{aligned}
&\varepsilon^2\left(ab\partial_X R + a\rho_c^2 V'(\rho_c)\partial_X R\right) \\
&+\varepsilon^3\Bigg(b^2 + \frac{a\rho_c^2 V'(\rho_c)}{2} - a\left|\rho_c^2 V'(\rho_c)\right| \\
&\times \gamma(\rho_c)\partial_X^2 R - b^2\tau_0\lambda a\Bigg)\partial_X^2 R \\
&+\varepsilon^4\left(\begin{array}{l}
(1-\lambda)\,a\partial_T R(\dfrac{a\rho_c^2 V'(\rho_c)}{6} + \dfrac{a\rho_c^2 V'''(\rho_c)}{6} \\
-\dfrac{\lambda a\left|\rho_c^2 V'(\rho_c)\right|\gamma(\rho_c)\left(1 + 3b^2\tau_0^2 + b^3\tau_0^3\right)}{3} \\
+\dfrac{\lambda a b^3\tau_0^2}{2} - \left|\rho_c^2 V'(\rho_c)\right|\gamma(\rho_c)\, b\lambda a)\partial_X R^3
\end{array}\right) \\
&+\varepsilon^5\left(\begin{array}{l}
(1-\lambda a\tau_0)\,2b\partial_{XT}R + \dfrac{a\rho_c^2 V'(\rho_c)}{24}\partial_X^4 R \\
+\dfrac{a\rho_c^2 V'''(\rho_c)}{12}\partial_X^2 R^3 - \dfrac{(1-\lambda)\,a}{12}\partial_X^4 R - \dfrac{\lambda a b^4\tau_0^3}{6}\partial_X^4 R \\
-\dfrac{\lambda a\left|\rho_c^2 V'(\rho_c)\right|\gamma(\rho_c)\left(1 + 6b^2\tau_0^2\right)}{12}\partial_X^4 R
\end{array}\right) \\
&= 0
\end{aligned} \tag{22}$$

where $V' = \frac{\partial V(\rho)}{\partial \rho}\big|_{\rho=\rho_c}$ and $V''' = \frac{\partial^3 V_0(\rho)}{\partial \rho^3}\big|_{\rho=\rho_c}$. Moreover, there is $a_c = \left(1 + \varepsilon^2\right)a$ at the critical point (ρ_c, a_c).

TABLE 1. The coefficients g_i of the model.

Symbol	Expression
g_1	$\frac{a\rho_c^2 V'(\rho_c)}{6}+\frac{\lambda a b^3 \tau_0^2}{2}-ab\lambda\left\|\rho_c^2 V'(\rho_c)\right\|\gamma(\rho_c) -\frac{\lambda a\left\|\rho_c^2 V'(\rho_c)\right\|\gamma(\rho_c)(1+3b^2\tau_0^2+b^3\tau_0^3)}{3}$
g_2	$\frac{a\rho_c^2 V'''(\rho_c)}{6}$
g_3	$\rho_c^4 (V'(\rho_c))^2$
g_4	$+\frac{a\rho_c^2 V'(\rho_c)}{24}-\frac{\lambda a b^4\tau_0^3}{6}-\frac{(1-\lambda)a}{12} -\frac{\lambda a\left\|\rho_c^2 V'(\rho_c)\right\|\gamma(\rho_c)(1+6b^2\tau_0^2)}{12}$
g_5	$\frac{a\rho_c^2 V'''(\rho_c)}{12}$

Besides, for the purpose of eliminating the second term of ε in the Eq. (20), we let the coefficient of the quadratic term of ε be equal to zero and get $b = -\rho_c^2 V'(\rho_c)$. Furthermore, substituting $a_c = (1+\varepsilon^2)a$ and $b = -\rho_c^2 V'(\rho_c)$ into Eq. (22), an evolutionary equation with only fourth and fifth terms of ε can be deduced as below:

$$\begin{aligned}&\varepsilon^4(-g_1\partial_X^3 R + g_2\partial_X R^3 + \partial_T R)\\&\quad+\varepsilon^5(g_4\partial_X^4 R + g_5\partial_X^2 R^3 + g_3\partial_X^2 R) = 0\end{aligned} \tag{23}$$

where the coefficients $g_i\,(1, 2, \ldots, 5)$ are shown in Table 1.

Because we want to derive the standard mKdV equation, we need to do the following equivalent substitution:

$$T = \frac{1}{g_1}T', \quad R = \sqrt{\frac{g_1}{g_2}}R' \tag{24}$$

Subsequently, substituting Eq. (24) into Eq. (23) and adding the correction term of $O(\varepsilon)$ into the model, the Eq. (23) is turned into

$$\partial_{T'}R' = \partial_X^3 R' - \partial_X R'^3 + \varepsilon M\left[R'\right] \tag{25}$$

where $M\left[R'\right] = \frac{g_3}{g_1}\partial_X^2 R' + \frac{g_4}{g_1}\partial_X^4 R' + \frac{g_5}{g_2}\partial_X^2 R'^3$ and this item means the higher order infinitesimal term.

In addition, after ignoring the correction term $O(\varepsilon)$, the kink-antikink density wave solution of the mKdV equation is

$$R_0'(X, T') = \sqrt{c}\tanh\left(\sqrt{\frac{c}{2}}(X - cT')\right) \tag{26}$$

where c denotes the propagation velocity of the above kink-antikink solitary wave.

Then, the following condition must be satisfied to help us obtain the value of the propagation velocity c for the kink solution:

$$(R_0', M[R_0']) = \int_{-\infty}^{+\infty} dX' R_0' M\left[R_0'\right] = 0 \tag{27}$$

where $M\left[R_0'\right] = M\left[R'\right]$, we get the general solution form of velocity c through solving the Eq. (27) as follows:

$$c = \frac{5g_2g_3}{2g_2g_4 - 3g_1g_5} \tag{28}$$

By replacing the velocity c in Eq. (26) with Eq. (28), we can get the following equation:

$$R(X, T) = \sqrt{\frac{g_1 c}{g_2}}\tanh\left(\sqrt{\frac{c}{2}}(X - cg_1T')\right) \tag{29}$$

Since then, the general kink-antikink solution of the mKdV equation can be expressed as

$$\rho_j(t) = \rho_c + \varepsilon\sqrt{\frac{g_1 c}{g_2}}\tanh\left(\sqrt{\frac{c}{2}}(X - cg_1T)\right) \tag{30}$$

Obviously, the amplitude A of the density soliton is:

$$A = \varepsilon\sqrt{\frac{g_1 c}{g_2}} \tag{31}$$

This kink-antikink soliton stands for the coexisting phases containing the freely moving phase with low density and the congested phase with high density. $\rho_j = \rho_c - A$ and $\rho_j = \rho_c + A$ are used to describe the densities of the freely moving phase and congested phase, respectively.

V. NUMERICAL SIMULATION

For convenience of numerical simulation, the Eq. (11) is rewritten into the following difference form:

$$\begin{aligned}&(1-\lambda a\tau_0)\left[\rho_j(t+2\Delta t) - 2\rho_j(t+\Delta t) + \rho_j(t)\right]\\&\quad + a\rho_0^2\Delta t^2\left[V(\rho_{j+1}) - V(\rho_j)\right] + a\Delta t\left[\rho_j(t+\Delta t) - \rho_j(t)\right]\\&\quad - (1-\lambda)a\Delta t^2\left|\rho_0^2 V'(\rho_0)\right|\left[\gamma(\rho_j)(\rho_{j-1}-\rho_j)\right.\\&\quad\left. -\gamma(\rho_{j+1})(\rho_j - \rho_{j+1})\right] - \lambda a\left|\rho_0^2 V'(\rho_0)\right|\Delta t^2\\&\quad\times\left(\begin{array}{l}\gamma(\rho_j(t-\tau_0))\left(\begin{array}{l}\rho_{j-1}(t) - \frac{\rho_{j-1}(t+\Delta t) - \rho_{j-1}(t)}{\Delta t}\\ -\rho_j(t-\tau_0)\end{array}\right)\\ -\gamma(\rho_{j+1}(t-\tau_0))(\rho_j(t-\tau_0) - \rho_{j+1}(t-\tau_0))\end{array}\right)\\&\quad - \left|\rho_0^2 V'(\rho_0)\right|\Delta t\\&\quad\times\left(\begin{array}{l}\gamma(\rho_j(t+\Delta t))(\rho_{j-1}(t+\Delta t) - \rho_j(t+\Delta t))\\ -\gamma(\rho_{j+1}(t+\Delta t))(\rho_j(t+\Delta t) - \rho_{j+1}(t+\Delta t))\\ -\gamma(\rho_j)(\rho_{j-1} - \rho_j) + \gamma(\rho_{j+1})(\rho_j - \rho_{j+1})\end{array}\right) = 0\end{aligned} \tag{32}$$

where Δt is the time step, and we set $\Delta t = 0.05$.

We select the following periodic boundary conditions and the initial conditions:

$$\rho_j(1) = \rho_j(0) = \begin{cases}\rho_0, & j \neq \frac{N}{2}, \frac{N}{2}+1,\\ \rho_0 - 0.05, & j = \frac{N}{2},\\ \rho_0 + 0.05, & j = \frac{N}{2}.\end{cases} \tag{33}$$

The parameters selected for numerical simulation are $N = 100$, $t = 10^4 s$, $\rho_0 = \rho_c = 0.5$, $a = 1.8$, $E = 10$.

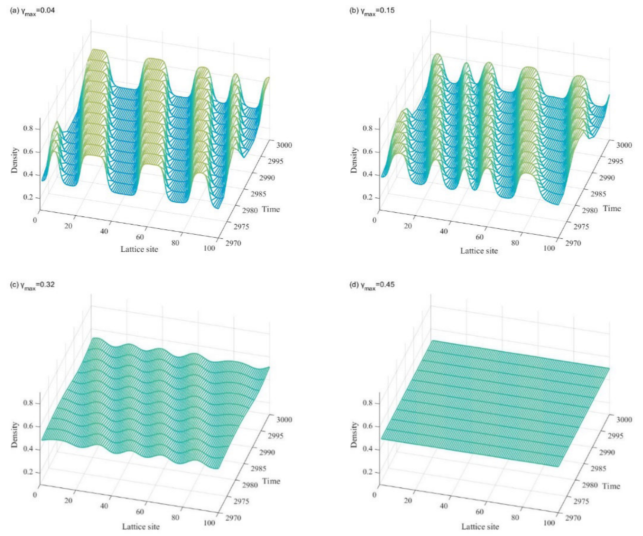

FIGURE 5. **The phase diagram of the model under different values of parameter γ_{max}.**

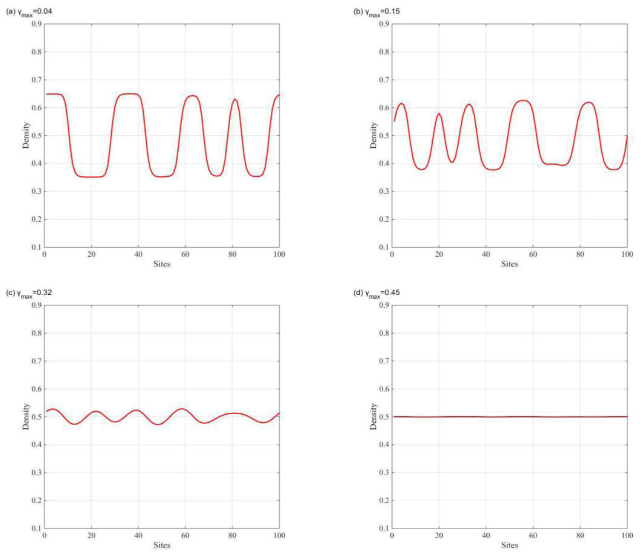

FIGURE 6. **The density profile at t = 10300s corresponds to Fig.5.**

Fig.5 depicts the propagation of initial disturbance under different γ_{max} with $\tau_0 = 0.1$ and $\lambda = 0.05$.When we set $\gamma_{max} = 0.04, 0.15, 0.32$, there are torque-reverse torque density waves in the Fig.5 (a), Fig.5 (b) and Fig.5 (c), because the stability condition is not satisfied. However, when the value of γ_{max} is selected as 0.45, the initial interference is gradually diluted over time, at which time the traffic flow restores to a stable state. Besides, we compare the overall trend of the four figures from Fig.5 (a) to Fig.5 (d), we can notice that the amplitude of density wave decreases with the increase of γ_{max}, which shows that the stability of the system can be enhanced by increasing the value of γ_{max} so as to alleviate traffic congestion.

Fig.6 shows the instantaneous traffic flow distribution at each lattice of Fig.5 at $t = 10300s$. In Fig.6 (a), the amplitude of the density wave is about 0.36-0.65, while Fig.6 (d) shows

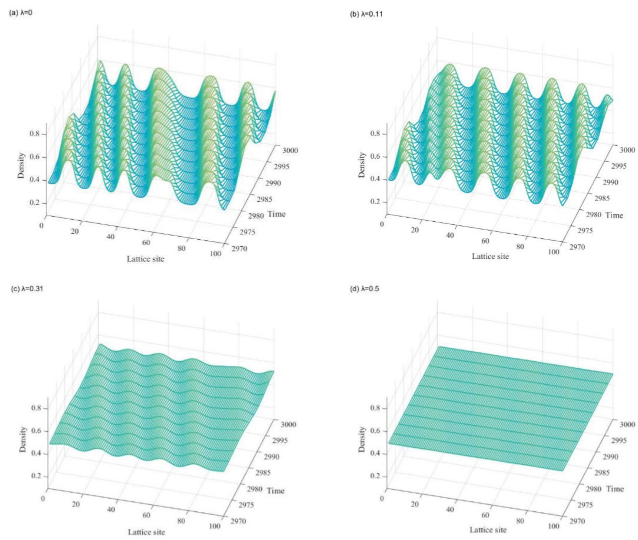

FIGURE 7. **The phase diagram of the model under different values of parameter λ.**

a straight line, that is, the amplitude becomes zero. Similarly, the amplitude of density wave motion decreases gradually with the increase of γ_{max} until it disappears. According to the above analysis, we can conclude that γ_{max} will drive the improvement of traffic flow stability.

Fig.7 shows the spatiotemporal evolution of density waves over a long enough period of time in the case of $\tau_0 = 0.1, \gamma_{max} = 0.2$. And the traffic patterns in Fig.7 (a), Fig.7 (b) and Fig.7 (c) are all unstable traffic flows, but with the increase of λ, the stability of traffic flow is gradually improved. In addition, In Fig.7 (d), the disturbance is absorbed and the traffic flow is uniform free flow throughout the space, because the parameters we set at this time satisfy the condition of traffic flow stability. To sum up, the self-stabilization can effectively improve traffic flow stability.

Fig.8 gives the density distribution corresponding to Fig.7 when $t = 10300s$. Obviously, the form of density wave in Fig.8 (c) is not as obvious as that in Fig.8 (a) and Fig.8 (b). And when we let $\lambda = 0.5$, The image becomes a straight line, which means that the system is stable and the density restores to the initial uniform flow. Similarly, the above results also reflect that the self-stabilization effect helps to stabilize traffic flow.

Fig.9 is the phase diagram of the model under different values of parameter τ_0.The degree of traffic congestion in Fig.9 (a), Fig.9 (b) and Fig.9 (c) is different. The most serious one is in Fig.9 (a). With the increase of τ_0, traffic flow congestion is obviously alleviated in Fig.9 (b) and Fig.9 (c). When the τ_0 is further increased to 0.45, traffic congestion does not occur, as shown in Fig.9 (d). Based on the above simulation results, considering the historical time τ_0, the stability of traffic flow can indeed be increased.

Finally, what is described in Fig.10 are the profiles of density corresponding to Fig.9. In Fig.10 (a), the range of density wave fluctuation is 0.4-0.6. With the increasing of τ_0, the fluctuation amplitude of density wave decreases gradually,

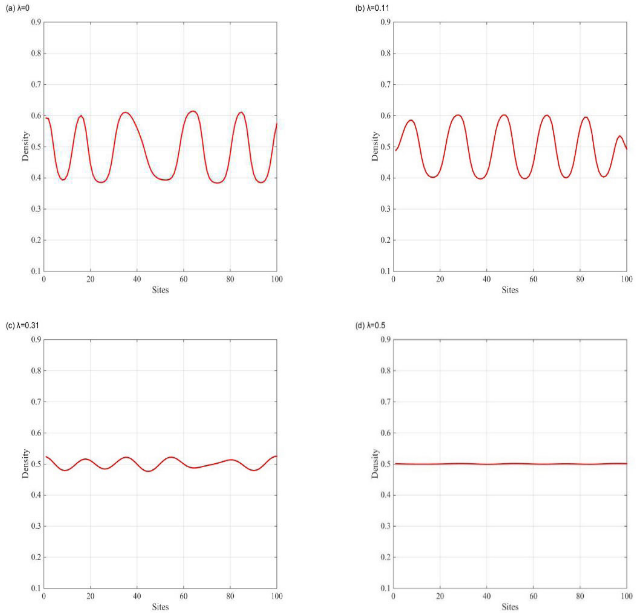

FIGURE 8. The density profile at t = 10300s corresponds to Fig.7.

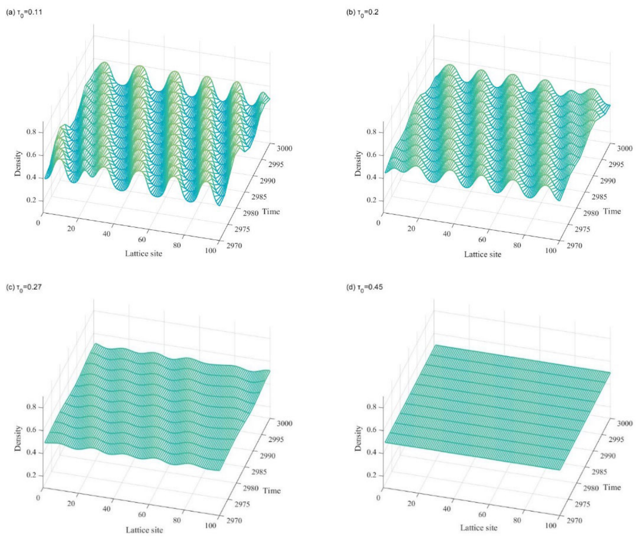

FIGURE 9. The phase diagram of the model under different values of parameter τ_0.

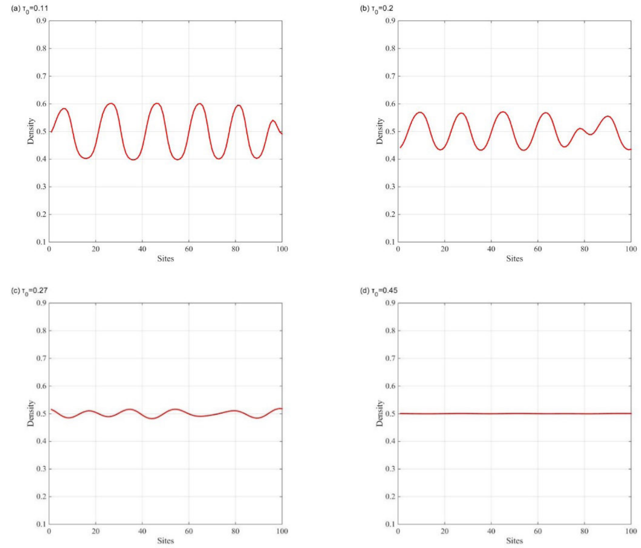

FIGURE 10. The density profile at t = 10300s corresponds to Fig.9.

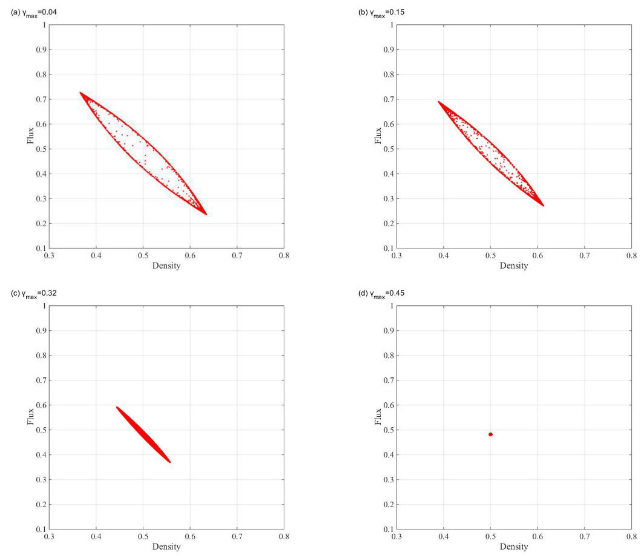

FIGURE 11. The hysteresis loops of traffic flux and density for different γ_{max}.

and all of them fluctuate around the initial density, which demonstrates that τ_0 cause a positive impact on the stability of traffic flow.

In the actual traffic, when the vehicle accelerates, it can't accelerate to the expected speed immediately, but when it decelerates, it can reduce the speed quickly. Therefore, the acceleration and deceleration of traffic flow in congested area will produce acceleration delay because acceleration force is generally weaker than deceleration force. And hysteresis loop is the main reason to induce traffic flow to reduce stability. What's more, the stronger the hysteresis loop effect is, the greater the disturbance to the steady traffic flow will be. And the following three groups of graphs describe the hysteresis loops of the relationship between flow and density under different parameters.

Fig.11 describes the hysteresis loops of traffic flux and density for different coefficients of $\gamma_{\max} = 0.04, 0.15, 0.32, 0.45$, respectively. We can intuitively find that the size of the hysteresis loop decreases with the increase of the value of $\gamma_{\max}$. As we can see, when the $\gamma_{\max}$ equals 0.45, the Fig.11 (d) shows a point, which means the hysteresis loop disappears and the traffic flow system is stable. Therefore, through the above analysis, we can again conclude that the empirical lane changing rate is conducive to promoting traffic flow stability.

Fig.12 are acquired through setting the different λ with the remaining parameters fixed. Fig.12 (a) depicts hysteresis loop when $\lambda = 0$, that is, without consider-

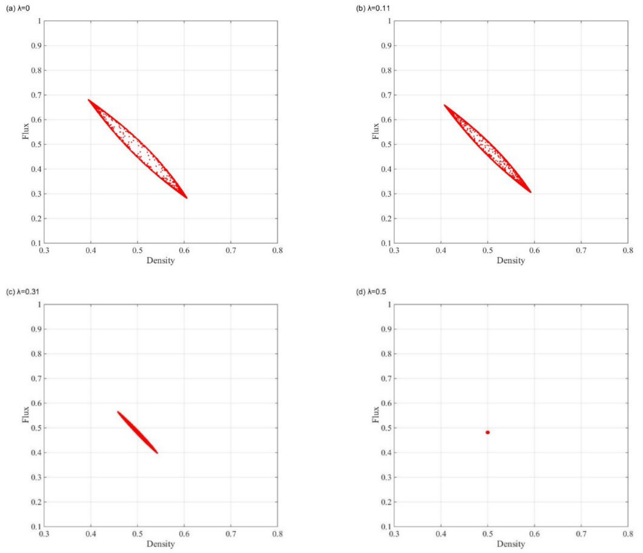

FIGURE 12. The hysteresis loops of traffic flux and density for different λ.

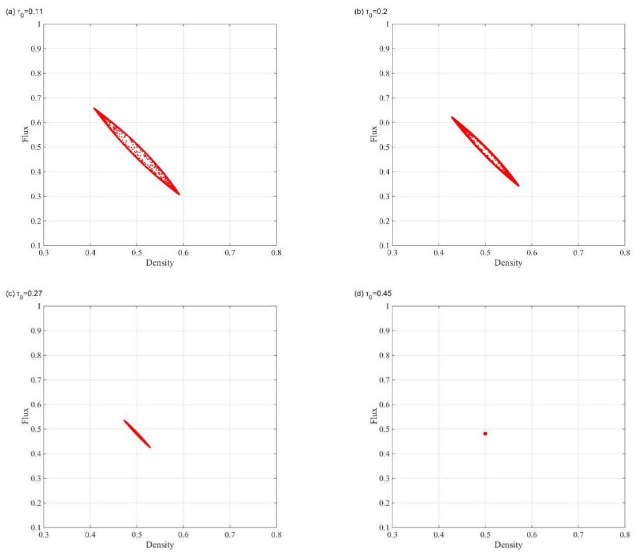

FIGURE 13. The hysteresis loops of traffic flux and density for different τ_0.

ing the self-stabilization effect. By comparing Fig.12 (a) and Fig.12 (b), it can be found that the traffic flow stability of lattice model with self-stabilization effect is better than that without self-stabilization effect. When λ increases to 0.5, there only exists one point, which indicated that traffic flow returns to uniform traffic flow. On the whole, the area of hysteresis loop decreases as the value of λ increases. Thus, we learn that the self-stabilization effect can alleviate traffic pressure to a certain extent.

Fig.13 is used to illustrate how the historical time τ_0 influence the traffic flow stability. It is precisely because the stability conditions of traffic flow are not satisfied that hysteresis loops appear in Fig.13 (a), Fig.13 (b) and Fig.13 (c), and the size of these hysteresis loops is slowly decreasing with the increase of τ_0. In addition, when τ_0 further increases to 0.45, the hysteresis loop disappears and the traffic flow becomes stable. In general, the historical time τ_0 can restrain traffic congestion and improve the stability of traffic flow.

VI. CONCLUSION

This paper presents a modified two-lane lattice hydrodynamic model, which accounting for the impact of the empirical lane changing rate and the self-stabilization effect. For the purpose of getting the linear stability condition, we make a linear analysis of the model, and the results reveal that both the empirical lane changing rate and the self-stabilization effect play an active role in traffic flow stability. Later, near the critical point, we derive the mKdV equation describing traffic congestion and obtain the kink-antikink solution of the equation. Besides, we use phase diagrams to illustrate the role of the empirical lane changing rate and the self-stabilization effect in improving traffic flow stability. The numerical simulation results are in agreement with the theoretical analysis. To sum up, the model established in this paper is close to the actual traffic, we can draw a reasonable conclusion that the traffic flow stability can be improved by taking the empirical lane changing rate and the self-stabilization effect into account. Considering the empirical lane changing rate, the stability of traffic flow is still closely related to the self-stabilization effect of current lattice's historical flow. Furthermore, whether increasing the coefficient of self-stabilization effect or increasing the historical time, it can promote the stability of traffic flow. This new model has some reference significance to solve the realistic traffic congestion.

REFERENCES

[1] C. Ma, W. Hao, A. Wang, and H. Zhao, "Developing a coordinated signal control system for urban ring road under the vehicle-infrastructure connected environment," *IEEE Access*, vol. 6, pp. 52471–52478, 2018.
[2] C. Ma, W. Hao, R. He, X. Jia, F. Pan, J. Fan, and R. Xiong, "Distribution path robust optimization of electric vehicle with multiple distribution centers," *PLoS ONE*, vol. 13, no. 3, 2018, Art. no. e0193789.
[3] C. Ma, W. Hao, F. Pan, and W. Xiang, "Road screening and distribution route multi-objective robust optimization for hazardous materials based on neural network and genetic algorithm," *PLoS ONE*, vol. 13, no. 6, 2018, Art. no. e0198931.
[4] C. Ma, R. He, and W. Zhang, "Path optimization of taxi carpooling," *PLoS ONE*, vol. 13, no. 8, 2018, Art. no. e0203221.
[5] W.-X. Zhu and L.-D. Zhang, "Analysis of car-following model with cascade compensation strategy," *Phys. A, Stat. Mech. Appl.*, vol. 449, pp. 265–274, May 2016.
[6] Z. Wen-Xing and Z. Li-Dong, "A new car-following model for autonomous vehicles flow with mean expected velocity field," *Phys. A, Stat. Mech. Appl.*, vol. 492, pp. 2154–2165, Feb. 2018.
[7] W.-X. Zhu and H. M. Zhang, "Analysis of mixed traffic flow with human-driving and autonomous cars based on car-following model," *Phys. A, Stat. Mech. Appl.*, vol. 496, pp. 274–285, Apr. 2018.
[8] W.-X. Zhu, D. Jun, and L.-D. Zhang, "A compound compensation method for car-following model," *Commun. Nonlinear Sci. Numer. Simul.*, vol. 39, no. 10, pp. 427–441, Oct. 2016.
[9] Y. Sun, H. Ge, and R. Cheng, "An extended car-following model considering driver's memory and average speed of preceding vehicles with control strategy," *Phys. A, Stat. Mech. Appl.*, vol. 521, pp. 752–761, May 2019.
[10] H. Ou and T.-Q. Tang, "An extended two-lane car-following model accounting for inter-vehicle communication," *Phys. A, Stat. Mech. Appl.*, vol. 495, no. 1, pp. 260–268, Apr. 2018.
[11] T.-Q. Tang, Y.-X. Rui, J. Zhang, and H.-Y. Shang, "A cellular automation model accounting for bicycle's group behavior," *Phys. A, Stat. Mech. Appl.*, vol. 492, pp. 1782–1797, Feb. 2018.

[12] T.-Q. Tang, X.-F. Luo, J. Zhang, and L. Chen, ''Modeling electric bicycle's lane-changing and retrograde behaviors,'' *Phys. A, Stat. Mech. Appl.*, vol. 490, pp. 1377–1386, Jan. 2018.
[13] T.-Q. Tang, J. Zhang, and K. Liu, ''A speed guidance model accounting for the driver's bounded rationality at a signalized intersection,'' *Phys. A, Stat. Mech. Appl.*, vol. 473, pp. 45–52, May 2017.
[14] X. Wu, X. Zhao, H. Song, Q. Xin, and S. Yu, ''Effects of the prevision relative velocity on traffic dynamics in the ACC strategy,'' *Phys. A, Stat. Mech. Appl.*, vol. 515, pp. 192–198, Feb. 2019.
[15] R. Cheng, H. Ge, and J. Wang, ''KdV–Burgers equation in a new continuum model based on full velocity difference model considering anticipation effect,'' *Phys. A, Stat. Mech. Appl.*, vol. 481, pp. 52–59, Sep. 2017.
[16] R. Cheng, H. Ge, and J. Wang, ''An extended continuum model accounting for the driver's timid and aggressive attributions,'' *Phys. Lett. A*, vol. 381, no. 15, pp. 1302–1312, 2017.
[17] R. Cheng, H. Ge, and J. Wang, ''An extended macro traffic flow model accounting for multiple optimal velocity functions with different probabilities,'' *Phys. Lett. A*, vol. 381, no. 32, pp. 2608–2620, 2017.
[18] Q. Zhai, H. Ge, and R. Cheng, ''An extended continuum model considering optimal velocity change with memory and numerical tests,'' *Phys. A, Stat. Mech. Appl.*, vol. 490, pp. 774–785, Jan. 2018.
[19] R. Cheng, H. Ge, and J. Wang, ''The nonlinear analysis for a new continuum model considering anticipation and traffic jerk effect,'' *Appl. Math. Comput.*, vol. 332, pp. 493–505 Sep. 2018.
[20] C. Jiang, R. Cheng, and H. Ge, ''Effects of speed deviation and density difference in traffic lattice hydrodynamic model with interruption,'' *Phys. A, Stat. Mech. Appl.*, vol. 506, pp. 900–908, Sep. 2018.
[21] C. Jiang, R. Cheng, and H. Ge, ''An improved lattice hydrodynamic model considering the 'backward looking' effect and the traffic interruption probability,'' *Nonlinear Dyn.*, vol. 91, no. 2, pp. 777–784, 2017.
[22] C. Jiang, R. Cheng, and H. Ge, ''Mean-field flow difference model with consideration of on-ramp and off-ramp,'' *Phys. A, Stat. Mech. Appl.*, vol. 513, pp. 465–476, Jan. 2019.
[23] R. Cheng and Y. Wang, ''An extended lattice hydrodynamic model considering the delayed feedback control on a curved road,'' *Phys. A, Stat. Mech. Appl.*, vol. 513, pp. 510–517, Jan. 2019.
[24] T. Nagatani, ''Modified KdV equation for jamming transition in the continuum models of traffic,'' *Phys. A, Stat. Mech. Appl.*, vol. 261, pp. 599–607, Dec. 1998.
[25] G. Peng, X. Cai, C. Liu, and B. Cao, ''A new lattice model of traffic flow with the consideration of the honk effect,'' *Int. J. Mod. Phys. C*, vol. 22, no. 9, pp. 967–976, 2011.
[26] A. K. Gupta and P. Redhu, ''Analyses of driver's anticipation effect in sensing relative flux in a new lattice model for two-lane traffic system,'' *Phys. A, Stat. Mech. Appl.*, vol. 392, no. 22, pp. 5622–5632, Nov. 2013.
[27] T. Wang, Z. Gao, J. Zhang, and X. Zhao, ''A new lattice hydrodynamic model for two-lane traffic with the consideration of density difference effect,'' *Nonlinear Dyn.*, vol. 75, nos. 1–2, pp. 27–34, 2014.
[28] J. Zhou, Z.-K. Shi, and C.-P. Wang, ''Lattice hydrodynamic model for two-lane traffic flow on curved road,'' *Nonlinear Dyn.*, vol. 85, no. 3, pp. 1423–1443, 2016.
[29] Q. Wang, R. Cheng, and H. Ge, ''A new lattice hydrodynamic model accounting for the traffic interruption probability on a gradient highway,'' *Phys. Lett. A*, vol. 383, no. 16, pp. 1879–1887, 2019.
[30] T. Nagatani, ''Jamming transitions and the modified Korteweg–de Vries equation in a two-lane traffic flow,'' *Phys. A, Stat. Mech. Appl.*, vol. 265, nos. 1–2, pp. 297–310, 1999.
[31] C. Zhu, S. Zhong, and S. Ma, ''Two-lane lattice hydrodynamic model considering the empirical lane-changing rate,'' *Commun. Nonlinear Sci. Numer. Simul.*, vol. 73, pp. 229–243, Jul. 2019.
[32] H. Y. Lee, H.-W. Lee, and D. Kim, ''Origin of synchronized traffic flow on highways and its dynamic phase transitions,'' *Phys. Rev. Lett.*, vol. 81, pp. 1130–1133, Aug. 1998.
[33] Z. Li, X. Li, and F. Liu, ''Stabilization analysis and modified KdV equation of lattice models with consideration of relative current,'' *Int. J. Mod. Phys. C*, vol. 19, no. 8, pp. 1163–1173, 2008.
[34] G. Zhang, ''The self-stabilization effect of lattice's historical flow in a new lattice hydrodynamic model,'' *Nonlinear Dyn.*, vol. 91, no. 2, pp. 809–817, 2018.
[35] G. Peng, H. Zhao, and X. Li, ''The impact of self-stabilization on traffic stability considering the current lattice's historic flux for two-lane freeway,'' *Phys. A, Stat. Mech. Appl.*, vol. 515, pp. 31–37, Feb. 2019.

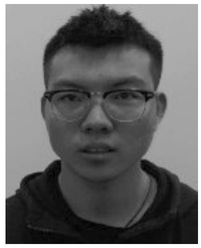

TING WANG was born in Lishui, Zhejiang, China, in 1996. He received the B.E. degree in traffic engineering from Jiangsu University, Zhenjiang, China, in 2018. He is currently pursuing the master's degree in port and waterway technology and management engineering with Ningbo University. His research focuses on traffic flow modeling and density wave analysis.

RONGJUN CHENG received the B.S. and M.S. degrees in math from Anhui Normal University, in 1999 and 2004, respectively, and the Ph.D. degree in mechanic from Shanghai University, in 2007. He is currently a Professor with Ningbo University. He has published more than 100 articles indexed by SCI. His research interests include traffic flow modeling, transportation safety, intelligent transportation systems, and meshless method.

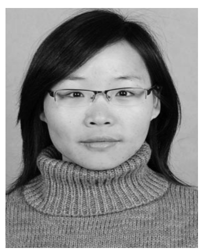

HONGXIA GE received the B.S. degree in traffic engineering from Anhui Normal University, in 2000, and the Ph.D. degree in transportation from Shanghai University, in 2013. She is currently a Professor with Ningbo University. She has published more than 100 articles indexed by SCI. Her researches focus on traffic flow modeling and density wave analysis.